Analysis of vapor-driven solutal Marangoni flows inside a sessile droplet

Junil Ryu[a], Junkyu Kim[a], Jonghyeok Park[a], Hyoungsoo Kim[a,*]

Department of Mechanical Engineering, KAIST, Daejeon 34141, South Korea

ARTICLE INFO

ABSTRACT

We study experimentally and theoretically how vapor-driven solutal Marangoni flows inside a sessile droplet are created. To measure the flow field, we perform a conventional particle image velocimetry (PIV). We show that the internal flow pattern can be controlled by the position and number of volatile liquid sources. To explain the mechanism, we develop a theoretical model based on Stokes flow, which predicts primary flow structures of experimental results. From the current study, we find two main conditions to determine the internal flow that are the distribution of the vapor molecules and the surface tension values depending on the concentration of the volatile liquid. From the analytical model, we successfully explain the mechanism of the solutal Marangoni flows induced by the volatile liquid components next to the sessile droplet, which can be used for optimization of the vapor-driven solutal Marangoni flow control and mixing.

© 2020 Elsevier Ltd. All rights reserved.

1. Introduction

Flow control inside a small droplet has actively been studied in various areas such as cell separation [1], inkjet printing [2,3], and bioassays [4,5]. For microfluidics technology, it should be low-cost, portable, easy to implement to the system. However, in general, complex and large devices are used to control and generate a flow pattern using external forces, for instance acoustic [6], electric [7], and magnetic force [8]. In a small volume, particularly, if there is a liquid-gas interface, surface tension effect becomes important compared to viscous, inertial, and gravitational effects. For this case, a Marangoni effect can be highly useful for controlling the flow patterns by using non-uniform distribution of surfactant [9–11], temperature [12–16], and solute [12,16–22]. According to the literature, it is introduced that the solutal Marangoni effect can be possibly applied for some biological applications because the volatile liquid components do not contaminate the sample and maintain a constant temperature while effectively generating flows and transporting materials [23].

Self-induced solutal Marangoni flows have been observed in an evaporating binary mixture droplet [24,25]. Recently, it is reported that Marangoni flows are generated while the volatile liquid evaporates next to the water drop, which were not controlled [20]. Later on, vapor-driven solutal Marangoni effects have been proposed for

a novel flow control and mixing method for micro-systems, which can be controlled by volatile liquid sources [21]. According to the literature, the velocity of the solutal Marangoni flow is proportional to the vapor pressure of the volatile liquid and the number of vortices (N) increases with the number of the source points (M), i.e., 2M = N. However, understanding of the mechanism of vapor-driven solutal Marangoni flows is still far from complete. For instance, as shown in Fig. 1, we observe that there is no flow pattern when we apply 4 source points of 3M Novec HFE-7000 to the droplet, where the vapor pressure of HFE-7000 is much higher than that of acetone [26,27], i.e. $v_{p_{(HFE-7000)}} = 52.7$ kPa $> v_{p_{(acetone)}} = 24.8$ kPa and the surface tension of HFE-7000 is lower than that of acetone [28,29], i.e. $\gamma_{HFE-7000} = 12.3$ mN/m $< \gamma_{acetone} = 23.2$ mN/m. Interestingly, if there is a single source of HFE-7000, there is a strong convection flow (see Supplementary Movie 1). Furthermore, for the multiple sources, it is still unclear that the reason of the vanishing of the flow pattern. We will try to explain this reason based on our experimental result and discussion. We expect that a relevant theoretical model could be useful to understand the mechanism.

In this study, we experimentally investigate the vapor-driven solutal Marangoni flow driven by vapor of a volatile liquid using particle image velocimetry (PIV). Based on the experimental observation, we assume that a primary flow is mostly a two-dimensional flow in polar coordinates. From this, we obtain an analytical model for the vapor-driven solutal Marangoni flow based on Stokes flow approximation in a sessile droplet. We observe that the theory predicts well the experimental results. Using the ana-

Nomenclature

v_p	vapor pressure (kPa)
R	droplet radius (mm)
h	droplet height (mm)
d	distance between droplet and source (mm)
d_0	capillary tube diameter (mm)
St	Stokes number
C	mole fraction
D	diffusion coefficient (m^2/s)
Pe	Peclet number
Re	Reynolds number
T	temperature ($^\circ$C)
μ	water dynamic viscosity (kg/(m $\cdot$ s))
γ	surface tension (mN/m)
ρ	density (kg/m^3)
τ	time (s)
τ_{Ma}	Marangoni stress (Pa)
ψ	stream function
ϵ	aspect ratio between droplet radius and height
ω	vorticity (1/s)

lytical model, we explain how solutal Marangoni flows are created and why the internal flow disappeared for multiple vapor sources, while changing the vapor distribution along the droplet interface by varying the boundary conditions of the mole fraction in the gas phase and the location of volatile liquid sources. We believe that the analytical model can be useful to optimize the vapor-driven solutal Marangoni flow controller and mixer for future microfluidics applications.

2. Experiments

In this study, to understand the working mechanism of vapor-driven solutal Marangoni flow, we performed a 2D conventional PIV and then we observed the depth-averaged flow pattern inside a flat droplet. In this sense, we focus on the 2D primary flow pattern in the middle of the droplet rather than a complicated three-dimensional flow structure near the edge of the droplet. We investigate the solutal Marangoni flows induced by volatile liquid (in this study, acetone) while changing the number and the position of source points. To measure the flow fields, we perform a conventional PIV that the experimental setup is illustrated in Fig. 2.
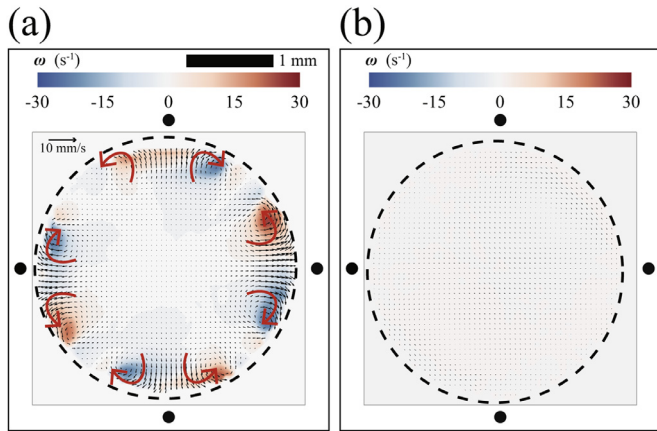

Fig. 1. Internal flow patterns of the vapor-driven solutal Marangoni flow induced by (a) 4 acetone source points and (b) 4 HFE-7000 source points. Black circle symbols indicate source locations that are equally apart from the droplet by 1 mm and the black dashed circle is the droplet contact line. The scale bar is 1 mm.

The detail experimental conditions are described in the following paragraphs.

2.1. Preparation of droplet and substrate

For experiments, a 2.0 μL droplet (de-ionized (DI) water, 18.2 MΩcm Merck Millipore, Direct-Q3) is deposited on a hydrophobic cover glass (Duran group, Germany) using a micropipette (Eppendorf, Germany). To pin the contact line, we partially change the surface condition. A PDMS mold that is punched to a circle shape at the center is attached on the cover glass and the substrate is treated with a BD-10AS high-frequency generator (Electro-Technic Products, USA) to make it hydrophilic. After the surface treatment, the PDMS mold is removed. When we deposit a liquid drop on the treated area, we observe that the contact line of the droplet pins and it remains a constant droplet radius, $R = 1.5 \pm 0.1$ mm. We also measured the droplet height, $h = 0.39 \pm 0.02$ mm, using the side view measurement.

2.2. Preparation of volatile liquid sources

A capillary tube (Sutter instrument, USA, $d_0 = 0.5$ mm) that contains acetone (density $\rho = 790$ kg/m^3, molar mass = 58.08 g/mol, surface tension $\gamma = 22.8$ mN/m, and vapor pressure $v_p = 24.6$ kPa at T = 20°C) is installed next to the sessile droplet to generate the vapor-driven solutal Marangoni flow, and its location is controlled with a linear stage by attaching on the tube holder as shown in Fig. 2(a). The acetone vapor diffused from the tip of the capillary tube alters the local surface tension of the droplet interface, and then the Marangoni stress generated as described in Fig. 2(b). To control the flow pattern, we vary the number of capillary tubes from 1 to 4 while keeping the same distance $d = 1$ mm. All experimental setups including the sessile droplet and capillary tubes are covered by the acrylic hood case (290 mm $\times$ 225 mm $\times$ 120 mm) to isolate from external convection effects (see Fig. 2).

2.3. Particle image velocimetry

To observe the flow inside the sessile droplet, we use fluorescence particles (PS-FlouRed-Fi320, microparticles GmbH, Germany) at a concentration of 12.5 $\times$ 10^{-5} wt%. In this experiment, the Stokes number ($St = \tau_p/\tau_l$) that is the ratio of the particle response time ($\tau_p = (1/18)\Delta\rho d_p^2/\mu \approx 10^{-8}$ s) and the time scale of the flow ($\tau_l = R/U \approx 10^{-1}$ s) is $O(10^{-7})$, where $\Delta\rho = (\rho_p - \rho_w)$ is the density difference between the particle density ρ_p (1050 kg/m^3) and the water density ρ_w (1000 kg/m^3), d_p is the particle diameter (1.9 μm), and μ is the dynamic viscosity of water. The primary flow velocity U is $O(10$ mm/s) obtained from the PIV measurement and R is the radius of the droplet. Thus, particles follow the flow well due to $St \ll 1$ [18]. The Nd:YAG laser (Microvec, China) stimulates the fluorescence particles and emitted fluorescent signals from particles are captured with a high-speed camera at the recording rate of 1000 frames per second.

Using iterative 2D cross-correlations of particles images with multiple interrogation windows (a half overlapping 64 $\times$ 64 pixels for a course grid and a half overlapping 32 $\times$ 32 pixels for a fine grid [30]), we obtain the velocity vectors. Furthermore, to improve the particle image quality, we use a contrast limited adaptive histogram equalization (CLAHE) and a high-pass filter. In this PIV results, the divergence error of the measurement results is estimated as [31],

$$\overline{\left(\frac{\partial u}{\partial x} + \frac{\partial v}{\partial y}\right)^2} \cong \left(\frac{2\sigma_{\Delta x}}{D_I \Delta t}\right)^2 \tag{1}$$

where $\sigma_{\Delta x}$ is the particle displacement, D_I is the interrogation window size. The error is between 0.050 and 0.396 pixels. Since
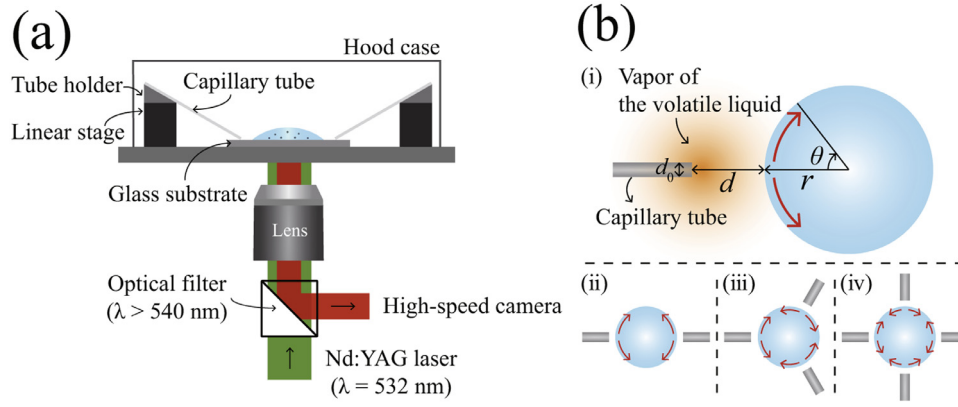
Fig. 2. (a) Schematic of the experimental setup for particle image velocimetry (PIV). During experiments, to exclude external convection effects, a sessile droplet and capillary tubes are covered by the hood case. For flow visualization, we used 1.9 μm fluorescence particles that emitted $\lambda = 607$ nm light when they are excited by $\lambda = 532$ nm laser. Fluorescent signals are captured by using an optical filter ($\lambda > 540$ nm) and a high-speed camera. (b) The top view of the vapor-driven solutal Marangoni flow experiments where the number of source points is (i) 1, (ii) 2, (iii) 3, and (iv) 4. Acetone vapor is diffused from a capillary tube. The distribution of the acetone vapor can be defined by the arrangement of capillary tubes containing acetone. The red arrow indicates the direction of the Marangoni stress induced by the acetone vapor. d_0 is the capillary diameter and d is the shortest distance between the capillary tip and the droplet surface.

the error is $\sim O(0.1$ pixels), we can assume that this error is consistent with a typical measurement uncertainty reported for the previous results [31,32].

3. Results, theoretical model, and discussion

In this section, to understand the experimental results, we develop a theoretical model for the vapor-driven solutal Marangoni flow in a sessile droplet. By comparing experimental and theoretical results, we show two dominant factors to determine the internal flow pattern. Finally, we explain the reason why different flow patterns can be observed although volatile liquid's vapors applied to the water droplet (see Fig. 1). Furthermore, we present unexpected vapor-driven solutal Marangoni flows by using experiments and theory.

3.1. Experimental result and discussion

We investigate the vapor-driven solutal Marangoni flow inside a sessile droplet by increasing the number of acetone sources, as shown in Fig. 3 (a). The black arrows are velocity vectors and the red arrows represent a typical flow structure. In this case, we observe that initially the internal flow monotonically develops in time after installing the acetone vapor source. For the acetone case, after 3 minutes, the flow pattern becomes quasi-steady. Therefore, to avoid the unsteady effect, in this study, we only consider and measure the flow field after 3 minutes. This flow development is already observed and explained in the preceding work (Park et al. [21]). In addition, we note that weak three-dimensional flow patterns near the contact line are observed, which is negligible compared to the primary flow pattern (the red arrows in Fig. 3 (a)).

We install the capillary tube containing volatile liquid on the substrate (see Fig. 2). Fig. 3 (a) shows that the number of circulating flows increases with the number of the sources. The flows are generated due to the solutal Marangoni stresses along the interface by the diffused acetone vapor. If the droplet surface is close to a source point (i.e., $\theta = 0$), there are more acetone vapors than other locations, so that the surface tension becomes lower at $\theta = 0$. Therefore, the Marangoni stress is directed from the close ($\theta = 0$) to the far position ($\theta = \pi/2$) as shown in Fig. 2(b) and then the solutal Marangoni flow along the droplet interface is created in the same direction as shown in Fig. 3(a). Here, since the height of the droplet is smaller than the diameter of the capillary tube, the amount of the acetone vapor diffused from the tip of the cap-

illary tube along the vertical direction will be similar. Thus, the surface tension gradient in the vertical direction would be much smaller than the horizontal direction. Hence, we assume that the surface tension gradient along the azimuthal direction is dominant that mainly drives solutal Marangoni stresses.

The solutal Marangoni flow is observed using PIV, and time-averaged wall-normal vorticity $\bar{w} = \left(\frac{\partial \bar{v}}{\partial x} - \frac{\partial \bar{u}}{\partial y} \right)$ is calculated with the time-averaged velocity ($\bar{u}$, $\bar{v}$) in cartesian coordinates. We observe that the magnitude and the size of vortices decreased with the number of sources. To understand this result, it is important to know the exact boundary condition, i.e., the surface tension gradient depending on the vapor concentration. However, unfortunately, it is extremely difficult to measure the Marangoni stress at the interface directly. Therefore, we try to develop an analytical model for this problem, which can be useful to understand the mechanism of the solutal Marangoni flows driven by the vapor of the volatile liquid component.

3.2. Analytical model for vapor-driven solutal Marangoni flow

In this problem, the acetone vapor is continuously propagated from the tip of the capillary tube to the water droplet surface, which is driven by diffusion. The diffusion time scale for this can be scaled as $\tau_d \sim d^2/D$, where D (10.5×10^{-6} m^2/s) is the diffusion coefficient of acetone in air [33]. After the acetone vapor arrives at the droplet interface, the attached acetone vapors generate Marangoni stresses and the vapors are followed by the Marangoni convective flow in a finite time $\tau_a \sim R/U_a$, where the flow velocity U_a is $O(10$ mm/s). Then, here, for the outside of the droplet, the Peclet number, $Pe_{out} = \tau_d/\tau_a = \frac{d^2}{R} \cdot \frac{U_a}{D}$, is order of unity, so that we can assume that the acetone vapor absorbs into the droplet interface [34]. Furthermore, for this particular case, the rate of diffusion inside the sessile droplet τ'_d is scaled as R^2/D, where D (1.2×10^{-9} m^2/s) is the diffusion coefficient of acetone in water [35], so the Peclet number inside the droplet, $Pe_{in} = \tau'_d/\tau_a \gg 1$, is much larger than unity. Thus, we can assume that the convection effect caused by the surface tension gradient is dominant in comparison to diffusion [36], and hence the solutal Marangoni circulating flow brings a pure DI water to the interface and therefore the Marangoni flow is continuously generated until the volatile liquid component is saturated [23].

In this problem, we assume that the in-plane two-dimensional flow inside the droplet is predominant because $Re \cdot \epsilon$ ($Re =$
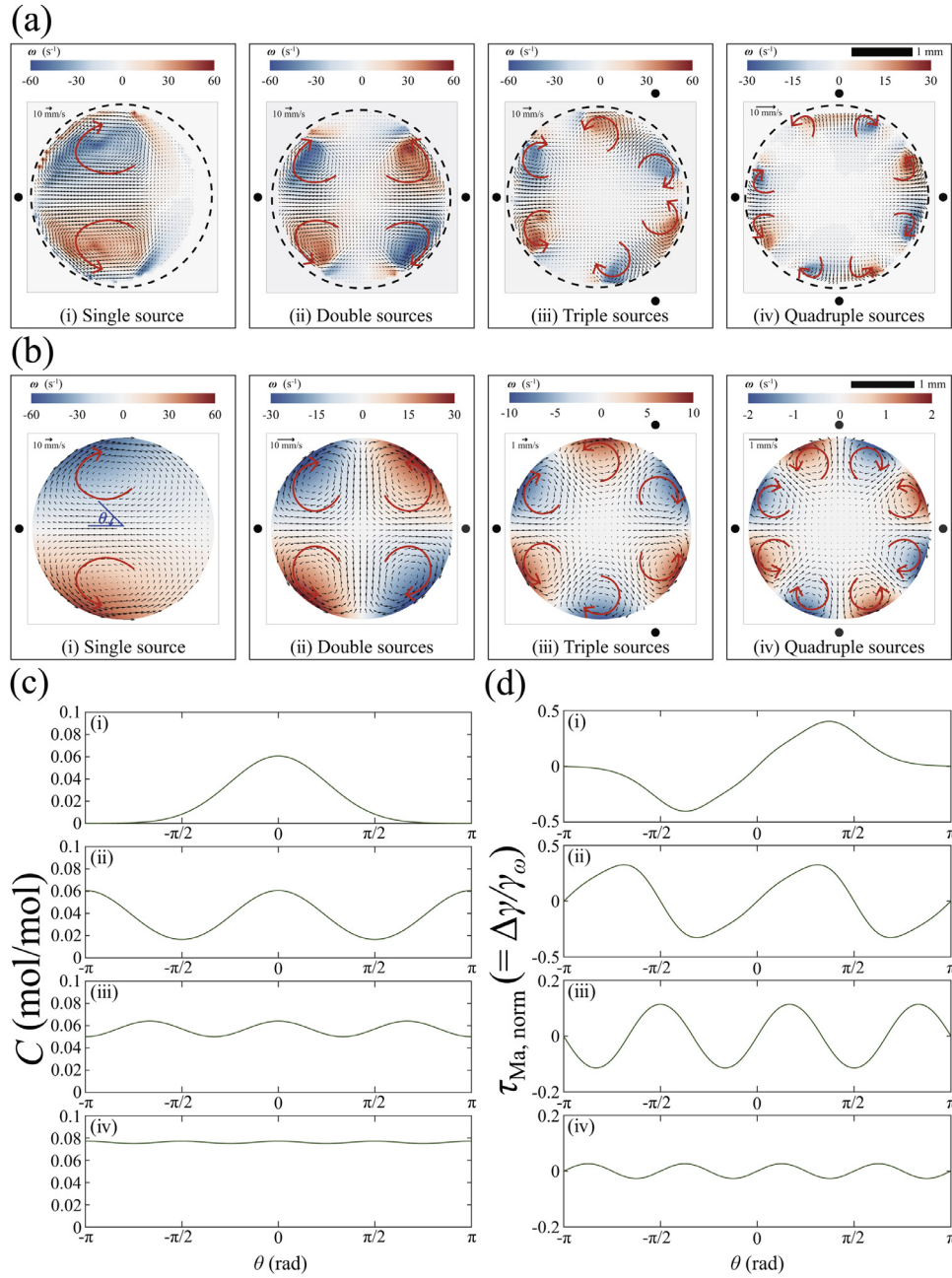
Fig. 3. (a) Experimental and (b) analytical results for the velocity vectors (black arrows) and vorticity (color map) of vapor-driven solutal Marangoni effects by varying the volatile liquid source point from 1 to 4 where $R = 1.5$ mm and $d = 1.0$ mm, respectively. In this case, we consider the solutal Marangoni flow caused by acetone sources. The black circle symbol indicates the position of the acetone source point, and the red arrows show a typical flow pattern inside a droplet. Boundary conditions for the analytical model: (c) The acetone mole fraction and (d) the normalized Marangoni stress ($\tau_{\text{Ma, norm}} = \Delta\gamma/\gamma_w$) along the droplet interface ($-\pi \leq \theta < \pi$) where γ_w is the surface tension of water. The scale bar is 1 mm.

$\rho_w UR/\mu$, $\epsilon = h/R \ll 1$; h is the height of the droplet) is smaller than unity due to a relatively flat shape of the droplet. Therefore, we simplify the system as a circular domain, so we assume that the two-dimensional flow is pre-dominant and it is governed by the Stokes equation in polar coordinates. The governing equation reads to the biharmonic equation in polar coordinates,

$$\nabla^4 \psi(r, \theta) = 0, \tag{2}$$

where $\psi(r, \theta)$ is the stream function and there is a general Fourier series solution to biharmonic equation, so-called Michell's solution [37]. To obtain the solution we apply five boundary conditions, i.e. (1) the periodicity of the stream function and velocity field ($\psi(r, \theta) = \psi(r, 2\pi + \theta)$, $u_{r,\theta}(r, \theta) = u_{r,\theta}(r, 2\pi + \theta)$), (2)

no velocity divergence at the center from the physical observation ($\nabla\psi(0, \theta) = 0$), (3) mass conservation ($\nabla^2\psi = 0$), (4) the kinematic boundary condition along the contact line ($u_r(R, \theta) = 0$), and (5) symmetric azimuthal velocity due to geometry ($u_\theta(r, \theta) = -u_\theta(r, -\theta)$, $u_r(r, \theta) = u_r(r, -\theta)$). As a result, the stream function and velocity vectors are, respectively,

$$\psi(r, \theta) = \sum_1^\infty B_{n1} r^n (r^2 - R^2) \sin n\theta, \tag{3}$$

$$u_r(r, \theta) = \sum_1^\infty n r^{n-1} B_{n1} (r^2 - R^2) \cos n\theta, \tag{4}$$

$$u_\theta(r, \theta) = -\sum_1^\infty B_{n1} r^{n-1} ((n+2)r^2 - nR^2) \sin n\theta, \tag{5}$$

where B_{n1} coefficients can be obtained from the Marangoni stress boundary condition from the following equation, Eq. (6). Here, we can assume that the Marangoni stress is equal to a viscous shear stress along the droplet interface due to $Re \cdot \epsilon \ (\sim 10^{-1}) \ < \ 1$ and $Ca (= \mu U / \Delta \gamma \sim 10^{-3}) \ \ll \ 1$,

$$\tau_{Ma} = \tau_{r\theta}|_{r=R} = \mu \left(\frac{1}{r} \frac{\partial u_r}{\partial \theta} + \frac{\partial u_\theta}{\partial r} - \frac{u_\theta}{r} \right) \Big|_{r=R}. \tag{6}$$

The Marangoni stress induced by the surface tension gradient ($\Delta \gamma$) can be scaled as

$$\tau_{Ma} \sim \frac{\Delta \gamma}{R}, \tag{7}$$

and by the chain rule the surface tension gradient can be written as

$$\Delta \gamma \approx \frac{\partial \gamma}{\partial C} \Big|_{C(\theta)} \frac{\partial C}{\partial \theta} \Big|_\theta \Delta \theta, \tag{8}$$

where C is the local concentration of the vapor of the volatile liquid components. As a result, by substituting Eqs. (3), (4), (5) for Eq. (6), we can get the stream function $\psi(r, \theta)$, radial velocity $u_r(r, \theta)$, and azimuthal velocity $u_\theta(r, \theta)$ as

$$\psi(r, \theta) = -\sum_{n=1}^\infty \left[\frac{1}{R} \int_0^{2\pi} \frac{\partial \gamma}{\partial C} \Big|_{C(\theta)} \frac{\partial C}{\partial \theta} \Big|_\theta \Delta \theta \sin n\theta d\theta \right]$$
$$\times \frac{r^n (r^2 - R^2)}{4\pi \mu n R^n} sin n\theta, \tag{9}$$

$$u_r(r, \theta) = -\sum_{n=1}^\infty \left[\frac{1}{R} \int_0^{2\pi} \frac{\partial \gamma}{\partial C} \Big|_{C(\theta)} \frac{\partial C}{\partial \theta} \Big|_\theta \Delta \theta \sin n\theta d\theta \right]$$
$$\times \frac{n r^{n-1} (r^2 - R^2)}{4\pi \mu n R^n} cos n\theta, \tag{10}$$

$$u_\theta(r, \theta) = \sum_{n=1}^\infty \left[\frac{1}{R} \int_0^{2\pi} \frac{\partial \gamma}{\partial C} \Big|_{C(\theta)} \frac{\partial C}{\partial \theta} \Big|_\theta \Delta \theta \sin n\theta d\theta \right]$$
$$\times \frac{((n+2) r^{n+1} - n R^2 r^{n-1})}{4\pi \mu n R^n} sin n\theta. \tag{11}$$

Furthermore, the vorticity ω is obtained from

$$\omega = -\nabla^2 \psi = \sum_{n=1}^\infty \left[\frac{1}{R} \int_0^{2\pi} \frac{\partial \gamma}{\partial C} \Big|_{C(\theta)} \frac{\partial C}{\partial \theta} \Big|_\theta \Delta \theta sin n\theta d\theta \right]$$
$$\frac{n+1}{\pi \mu n R^n} sin n\theta. \tag{12}$$

The velocity can be determined by the concentration distribution of the vapor ($\frac{\partial C}{\partial \theta}$) and the surface tension gradient depending on the concentration of the volatile liquid component ($\frac{\partial \gamma}{\partial C}$) if we fix the system including the working fluid, the source distance, and the droplet size.

3.3. Vapor distribution of volatile liquid

To estimate the Marangoni stress at the liquid-gas interface, the surface tension gradient along the droplet interface should be defined. Based on Eq. (8), we decomposite two parts: the surface tension value depending on concentration $\gamma(C)$ and the vapor concentration depending on the location $C(\theta)$. $\gamma(C)$ is directly measured by the pendant droplet method as shown in Fig. 4. However, it is difficult to measure $C(\theta)$ along the droplet surface, and therefore the vapor distribution of the volatile liquid along the droplet interface should be properly estimated.

In this problem, the vapor of acetone is purely diffused into air and then vapor distribution can be expressed as exponential function of time and distance based on Fick's second law. However, we
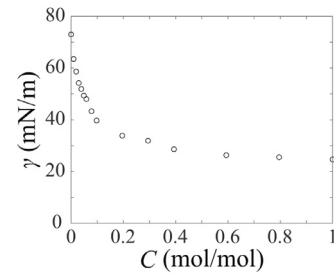
Fig. 4. Surface tension of an acetone-water mixture measured by the pendant droplet method where C is the normalized mole fraction of the acetone.

can neglect the time term because we observe the flow pattern at a quasi-steady regime around 3 min after exposing the sources. So for the sake of simplicity we assume that the vapor diffused with a Gaussian vapor distribution profile along the droplet interface,

$$C_A(\theta) = \frac{1}{\sigma \sqrt{2\pi}} \exp \left[-\frac{1}{2} \left(\frac{\theta - \theta_0}{\sigma} \right)^2 \right], \tag{13}$$

where σ is a standard deviation constant of Gaussian distribution and θ_0 is the azimuthal location aligned to the source point ($\theta = 0$). The acetone mole fraction in the vicinity of the contact line of the droplet assumed to be almost the same as that in air ($C(\theta) = C_A(\theta)$) because the acetone vapor can be absorbed to the liquid
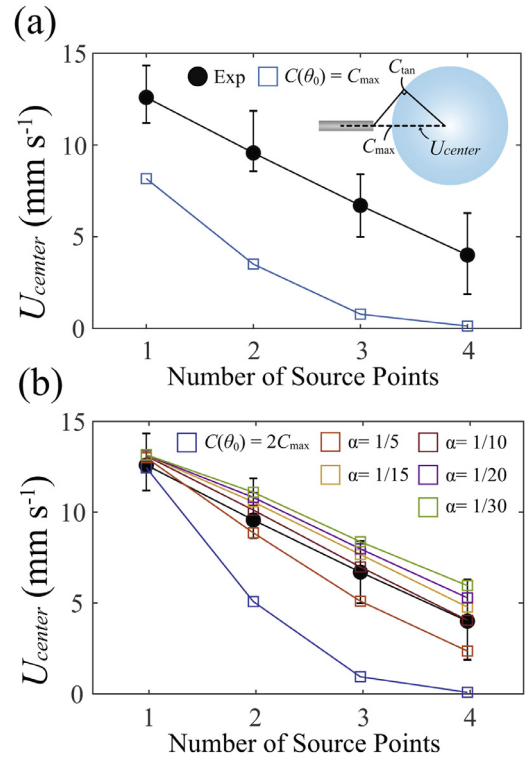
Fig. 5. Comparison of U_{center} aligned to the vapor source position (the capillary tube) between theory and experiments while the number of source points is varied from 1 to 4. (a) Black symbols from experiments and blue symbols are from the analytical model where C_{max} is from Eq. (15). The error bar indicates the range of velocity fluctuations in the quasi-steady regime. In this case, for the blue symbols, C_{tan}/C_{max} is assumed to be 1/2 from Eq. (15) and Park et al. [21], where C_{max} is the mole fraction at the point that is the closest from the source and C_{tan} indicates the mole fraction at the position that meets with the tangent line from the source on the interface of the droplet. The inset indicates the location of U_{center}. (b) Comparison of the effect of the prefactor α ($= C_{tan}/C_{max}$) for the vapor distribution where the C_{max} value is empirically obtained to match with experimental results, which is doubled as the previously determined condition (Eq. (15)). Here, the variation of α indicates the shape of the Gaussian distribution profile.
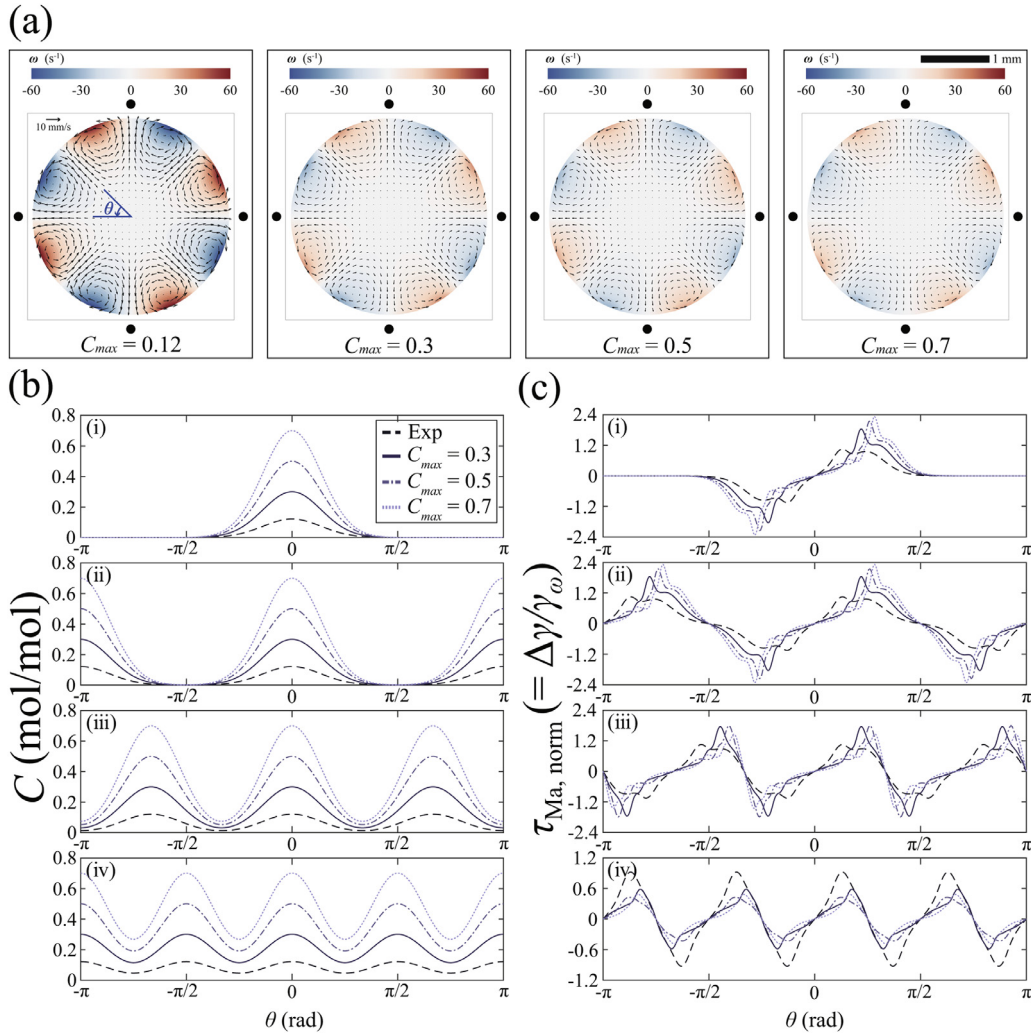
Fig. 6. (a) Comparison of internal flow patterns based on the theoretical model while increasing the maximum mole fraction (C_{max}). In this figure, we plot the case of 4 volatile liquid sources where the Marangoni stress decreases as the acetone mole fraction increases. Here, the condition, $C_{max} = 0.12$, is the best matched case with experimental results. The black circle symbol represents the position of acetone source points. (b) Profiles of the acetone mole fraction and (c) the normalized Marangoni stress where the number of source points is (i) 1, (ii) 2, (iii) 3, (iv) 4. The scale bar is 1 mm.

interface in a very short time [38]. To apply the Gaussian profile to our system, we defined the mole fraction at θ_0 which is the closest to the source point as C_{max} $(= C(\theta_0) = \frac{1}{\sigma\sqrt{2\pi}})$, and the mole fraction at the point which meets with the line that tangent to the surface of the droplet from the source point as $C_{tan} = C(\theta_1)$ where $\theta_1 = \cos^{-1}(R/(d+R))$, as shown in the inset of Fig. 5(a). From C_{max}, C_{tan}, and θ_1, the concentration profile along the vicinity of the droplet surface reads as

$$C(\theta) = C_{max} \exp\left(\frac{\theta}{\theta_1}\right)^2 \ln\left(\frac{C_{tan}}{C_{max}}\right), \tag{14}$$

where C_{max} and C_{tan} of the acetone mole fraction profile can be determined such as,

$$C_{max} = \frac{c_0 d_0}{2d} \quad \text{and} \quad C_{tan} = \frac{c_0 d_0}{2\sqrt{(d+R)^2 - R^2}}. \tag{15}$$

Here, c_0 is the saturated concentration that is the acetone mole fraction at the tip of the capillary tube, which is calculated by Dalton's law [39] based on the diffusion mechanism [21]. By defining the mole fraction, we obtain the analytical result from Eqs. (10)

and (11),

$$u_r(r,\theta) = -\sum_{n=1}^{\infty}\left[\frac{1}{R}\int_0^{2\pi} f(\theta)g(C)\Delta\theta \sin n\theta d\theta\right]$$
$$\times \frac{nr^{n-1}(r^2 - R^2)}{4\pi\mu nR^n}\cos n\theta, \tag{16}$$

$$u_\theta(r,\theta) = \sum_{n=1}^{\infty}\left[\frac{1}{R}\int_0^{2\pi} f(\theta)g(C)\Delta\theta \sin n\theta d\theta\right]$$
$$\times \frac{((n+2)r - nR^2r^{n-1})}{4\pi\mu nR^n}\sin n\theta, \tag{17}$$

where $f(\theta) = \frac{C(\theta)}{C_{max}} = \exp[(\frac{\theta}{\theta_1})^2 \ln(\frac{C_{tan}}{C_{max}})]$ and $g(C) = \frac{\partial\gamma}{\partial C}(\frac{2\theta C_{max}}{\theta_1^2})\ln(\frac{C_{tan}}{C_{max}})$. The analytical results for flow patterns are presented in Fig. 3(b) and the boundary conditions are described in Figs. 3(c) and 3(d).

For the single source, we use Eqs. (16) and (17) combined with the concentration condition Eq. (15). Then, for the multiple sources, the solution could be obtained by using superposition from the single source result because of linearity. We observe that the primary flow fields show a good agreement between theory

and experiments. Namely, the number of vortices increases with the number of sources and the typical flow pattern is also similar. However, the detail flow structure near the contact line is not perfectly matched. Possibly, this could be due to the three-dimensional effect that is already mentioned earlier and data post-processing. Furthermore, the magnitude of vorticity is lower than that of experiments. We suspect the actual local concentration of the acetone vapor might be different from what we expected from Eq. (15) and Park et al. [21].

To check the effect of the local vapor concentration on the result of the primary flow, we plot and compare the magnitude of the internal flow velocity at $\theta = 0$ aligned to the capillary tube, named as U_{center} (see the inset of Fig. 5(a)), by varying the number of volatile liquid sources (see the black symbols of Fig. 5). The error bars in Fig. 5 are from the minimum and maximum velocity due to the oscillatory flow pattern, which is already reported by Park et al. [21]. We also confirm that the periodically repeating flow patterns are quasi-steady. Based on Eq. (15) that is suggested from the preceding work, we plot the blue line in Fig. 5(a), which does not predict well the experimental results. As we discussed earlier, this might be due to the incorrect estimation for the vapor distribution along the droplet interface, which is not possible to measure directly for now. From Eqs. (16) and (17), the magnitude of velocity is affected by C_{max} and the ratio between C_{max} and C_{tan} at the same time. Therefore, we compare the U_{center} by changing C_{max} and the value α ($=C_{tan}/C_{max}$). In Fig. 5(b), we empirically find $C(\theta_0) = 2C_{max}$ to match the U_{center} between experiments and theory for one source where $\theta(0) = \theta_0$. The prefactor α determines the shape of the vapor distribution, which is tested and plotted in Fig. 5(b). In this problem, for $\alpha = 1/10$, the U_{center} of the analytical results show a good agreement with the experimental results. We admit that the analytical model might still be incomplete because of the unknown boundary condition, ($\partial C/\partial \theta$). Nevertheless, we should emphasize that the current analytical model possibly contributes to predict the primary flow patterns inside a sessile droplet, which can be used for the optimization of the solutal Marangoni effects as an effective flow controller in the near future.

3.4. Effects of boundary conditions on internal flow patterns

We show that the analytical results are qualitatively in good agreement with experimental results. It shows that the flow structure is determined from the interplay of the two effects: the surface tension gradient ($\frac{\partial \gamma}{\partial C}$) and the mole fraction profile ($\frac{\partial C}{\partial \theta}$) simultaneously. Typically, the surface tension value depending on a mixture ratio is measured by experiments, so that it can be predetermined. Then, it turns out that the internal flow pattern can be determined by the vapor concentration distribution of the volatile liquid. We observe that the effects of the vapor concentration distribution by changing the amount of a vapor and the source location on the internal flow patterns.

In the previous work, we reported that when the volatility of a volatile liquid source increases, a velocity of the solutal Marangoni flow becomes stronger [21]. In the same manner, we can imagine that if there are more vapors diffused into air (next to the droplet interface), the Marangoni stress should be increased. However, through the experimental result in Fig. 1(b), we observe that it is not always true. To clarify this result, we vary the C_{max} indicating the amount of a vapor and increase as 0.12, 0.3, 0.5, and 0.7 where $C_{max} = 0.12$ is the best matched case with current experimental results using acetone (see Fig. 5(b)). The analytical model shows that the magnitude of vorticity and velocity decreases with the concentration of the vapor, as shown in Fig. 6. In fact, this result can explain why the HFE-7000 case shows almost no flow pattern as presented in Fig. 1(b). Due to the large amount of the
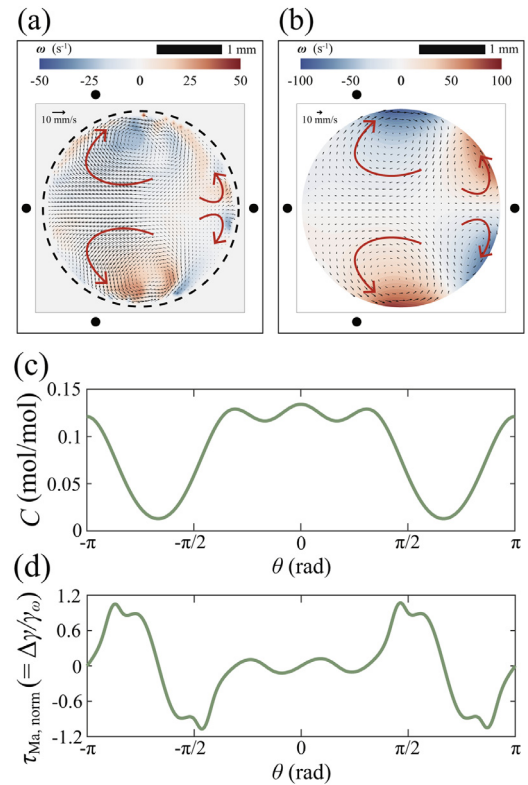

Fig. 7. (a) Experimental and (b) analytical results by changing the location of source points where $d = 1.0$ mm for 4 sources. The black circle symbol indicates the location of acetone source points, and the red arrows indicate a typical flow pattern inside a droplet. The scale bar is 1 mm. Boundary conditions for (c) the acetone vapor concentration and (d) the Marangoni stress along the droplet interface are presented, respectively. The scale bar is 1 mm.

vapor in the vicinity of the surface of the sessile droplet, the vapors of HFE-7000 cover the entire droplet and the concentration of the vapors is larger, so that the concentration gradient is decreased (namely, the Marangoni stress is decreased as well), as shown in Figs. 6(b) and 6(c).

To further investigate, based on the theoretical model, we examine the concentration profile and Marangoni stress along the droplet interface by increasing the number of sources. As the number of sources increases, the overlapped region of the acetone vapor increases where the local concentration is not zero, as shown in Fig. 6(b). Therefore, the magnitude of the Marangoni stress $\tau_{Ma, norm}$ decreases as shown in Fig. 6(c). For the vapor-driven Marangoni stress, the surface tension gradient $\frac{\partial \gamma}{\partial C}$ is important, rather than the magnitude of the local surface tension.

Additionally, we test whether the distribution of the vapor sources can affect to the Marangoni velocity and vorticity. Based on the current study (see Figs. 1, 3, and 6), 8 vortices should be induced by 4 source points. However, we observe that 4 vortices are generated by 4 source points experimentally and analytically as shown in Figs. 7(a) and 7(b). Since volatile liquid vapors from different sources are overlapped as shown in Fig. 7(c), the Marangoni stresses are almost zero at the overlapped region. This indicates that the internal flows can be dramatically changed by the location of source points. Furthermore, using the analytical model, we observe various flow patterns by tunning the boundary conditions as Fig. 8 (Experimental results of each case are presented in Fig. S1 of the Supplementary Information). For Fig. 8(a) case, by modifying the position of the sources, we obtain the higher magnitude of vorticity and velocity compared to the double and triple sources of Figs. 3(a) and 3(b) while keeping $d = 1$ mm. These examples
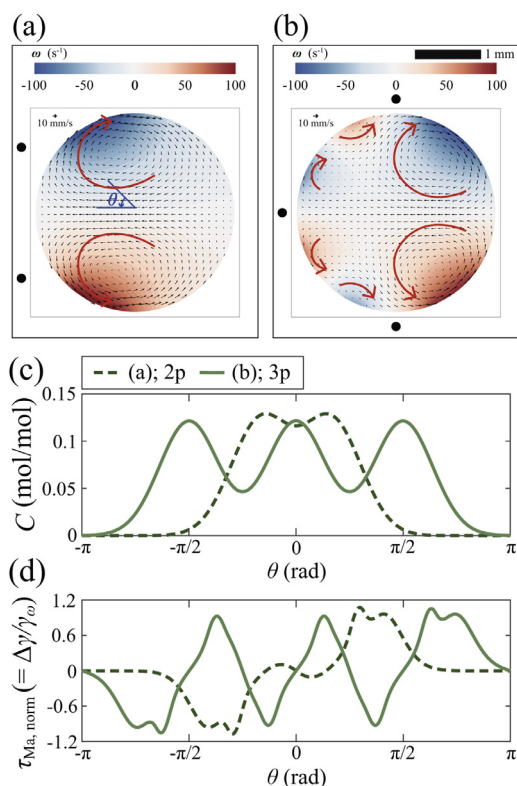
Fig. 8. Examples for unexpected internal flow patterns by changing the location and the number of source points where $d = 1.0$ mm for (a) 2 and (b) 3 sources. The black circle symbol indicates the location of acetone source points, and the red arrows indicate a typical flow pattern inside a droplet. Boundary conditions for (c) the acetone vapor concentration and (d) the Marangoni stress along the droplet interface are presented, respectively. The scale bar is 1 mm.

represent that the analytical model could be used for the optimization of the vapor-driven solutal Marangoni flow controller and mixer.

4. Conclusion

In this study, we investigate how the vapor-driven solutal Marangoni flow creates inside a sessile droplet. To explain this mechanism, we develop an analytical model based on the Stokes flow, which shows a good agreement with experimental results. Furthermore, the model clarifies why acetone and HFE-7000 sources provide a different flow pattern as shown in Fig. 1.

Using the analytical model, we demonstrate that the Marangoni stress is the result of interplays of surface tension values of a volatile liquid and a molecule distribution of the diffused vapor in the gas phase. It shows that the interference between the diffused vapors is also important to generate the vapor-driven solutal Marangoni flow. Based on this analytical model, we could consider and generate all the possible flow structures by applying boundary conditions and we expect that we can develop an optimization model if we can use a machine-learning model.

Experimentally, we could measure the surface tension values depending on the mole fraction using multiple methods. Unfortunately, for now, the vapor concentration of the volatile liquid component in the vicinity of the droplet interface was not measured. In this study, by comparing analytical results with experimental results, we estimated the vapor distribution. However, recently, using an optical interferometry method, the vapor cloud was visualized [26,40]. If this measurement technique can capture the molecule distribution of the diffused vapor in air, it could be

useful to understand the detail of the mechanism. Nonetheless, we believe that the current analytical model as a simulation tool could provide insights into the optimization and commercialization of solutal Marangoni flow controller and mixer.

Credit Author Statement

All persons who meet authorship criteria are listed as authors, and all authors certify that they have participated sufficiently in the work to take public responsibility for the content, including participation in the concept, design, analysis, writing, or revision of the manuscript. Furthermore, each author certifies that this material or similar material has not been and will not be submitted to or published in any other publication before its appearance in International Journal of Heat and Mass Transfer.

Authorship contributions

Hyoungsoo Kim and Junil Ryu conceived the project and planned the experiments. Junil Ryu carried out the experiments and obtained the theoretical model. Jonghyeok Park supported the experiments. Hyoungsoo Kim, Junkyu Kim, and Junil Ryu, analyzed the data and developed the theoretical analysis. Junil Ryu wrote the first draft of the manuscript. All authors discussed and edited the manuscript.

Declaration of Competing Interest

The authors declare that they have no known competing financial interests or personal relationships that could have appeared to influence the work reported in this paper.

Acknowledgement

Supplementary material

Supplementary material associated with this article can be found, in the online version, at doi:10.1016/j.ijheatmasstransfer.2020.120499.

References

[1] J.Y. Jung, H.Y. Kwak, Separation of microparticles and biological cells inside an evaporating droplet using dielectrophoresis, Analytical Chemistry 79 (13) (2007) 5087–5092.

[2] J. Park, J. Moon, Control of colloidal particle deposit patterns within picoliter droplets ejected by ink-jet printing, Langmuir 22 (8) (2006) 3506–3513.

[3] M. Kuang, L. Wang, Y. Song, Controllable printing droplets for high-resolution patterns, Advanced Materials 26 (40) (2014) 6950–6958.

[4] T.S. Wong, T.H. Chen, X. Shen, C.M. Ho, Nanochromatography driven by the coffee ring effect, Analytical Chemistry 83 (6) (2011) 1871–1873.

[5] R. Hernandez-Perez, Z.H. Fan, J.L. Garcia-Cordero, Evaporation-driven bioassays in suspended droplets, Analytical Chemistry 88 (14) (2016) 7312–7317.

[6] H. Li, J.R. Friend, L.Y. Yeo, Surface acoustic wave concentration of particle and bioparticle suspensions, Biomedical Microdevices 9 (5) (2007) 647–656.

[7] D. Mampallil, D. van den Ende, F. Mugele, Controlling flow patterns in oscillating sessile drops by breaking azimuthal symmetry, Applied Physics Letters 99 (15) (2011) 2009–2012.

[8] T.G. Kang, M.A. Hulsen, P.D. Anderson, J.M. Den Toonder, H.E. Meijer, Chaotic mixing induced by a magnetic chain in a rotating magnetic field, Physical Review E - Statistical, Nonlinear, and Soft Matter Physics 76 (6) (2007) 1–11.

[9] T. Still, P.J. Yunker, A.G. Yodh, Surfactant-induced Marangoni eddies alter the coffee-rings of evaporating colloidal drops, Langmuir 28 (11) (2012) 4984–4988.

[10] W. Sempels, R. De Dier, H. Mizuno, J. Hofkens, J. Vermant, Auto-production of biosurfactants reverses the coffee ring effect in a bacterial system, Nature Communications 4 (2013) 1–8.

[11] S.N. Varanakkottu, M. Anyfantakis, M. Morel, S. Rudiuk, D. Baigl, Light-directed particle patterning by evaporative optical Marangoni assembly, Nano Letters 16 (1) (2016) 644–650.

[12] M. Kaneda, Y. Takao, J. Fukai, Thermal and solutal effects on convection inside a polymer solution droplet on a substrate, International Journal of Heat and Mass Transfer 53 (21-22) (2010) 4448–4457.

[13] R.O. Grigoriev, Chaotic mixing in thermocapillary-driven microdroplets, Physics of Fluids 17 (3) (2005) 033601.

[14] J.R. Trantum, M.L. Baglia, Z.E. Eagleton, R.L. Mernaugh, F.R. Haselton, Biosensor design based on Marangoni flow in an evaporating drop, Lab on a Chip 14 (2) (2014) 315–324.

[15] J.D. Shephard, V.D. Ta, J. Li, E. Esenturk, R.W. Kay, T.J. Wasley, C. Connaughton, R.M. Carter, P.J. Smith, J. Stringer, Dynamically controlled deposition of colloidal nanoparticle suspension in evaporating drops using laser radiation, Soft Matter 12 (20) (2016) 4530–4536.

[16] J.-J. Yu, Y.-R. Li, J.-C. Chen, Y. Zhang, C.-M. Wu, Thermal-solutal capillary-buoyancy flow of a low prandtl number binary mixture with various capillary ratios in an annular pool, International Journal of Heat and Mass Transfer 113 (2017) 40–52.

[17] A. Cecere, C. Buffone, R. Savino, Self-induced marangoni flow in evaporating alcoholic solutions, International Journal of Heat and Mass Transfer 78 (2014) 852–859.

[18] H. Kim, J. Lee, T.H. Kim, H.Y. Kim, Spontaneous Marangoni Mixing of Miscible Liquids at a Liquid-Liquid-Air Contact Line, Langmuir 31 (31) (2015) 8726–8731.

[19] N.J. Cira, A. Benusiglio, M. Prakash, Vapour-mediated sensing and motility in two-component droplets, Nature 519 (7544) (2015) 446–450.

[20] O. Hegde, S. Chakraborty, P. Kabi, S. Basu, Vapor mediated control of microscale flow in sessile droplets, Physics of Fluids 30 (12) (2018) 122103.

[21] J. Park, J. Ryu, H.J. Sung, H. Kim, Control of solutal marangoni-driven vortical flows and enhancement of mixing efficiency, Journal of Colloid and Interface Science 561 (2020) 408–415.

[22] R. Malinowski, G. Volpe, I.P. Parkin, G. Volpe, Dynamic control of particle deposition in evaporating droplets by an external point source of vapor, The Journal of Physical Chemistry Letters 9 (3) (2018) 659–664.

[23] H. Kim, K. Muller, O. Shardt, S. Afkhami, H.A. Stone, Solutal marangoni flows of miscible liquids drive transport without surface contamination, Nature Physics 13 (11) (2017) 1105–1110.

[24] J.R. Christy, Y. Hamamoto, K. Sefiane, Flow transition within an evaporating binary mixture sessile drop, Physical Review Letters 106 (20) (2011) 205701.

[25] R. Bennacer, K. Sefiane, Vortices, dissipation and flow transition in volatile binary drops, Journal of Fluid Mechanics 749 (2014) 649–665.

[26] S. Dehaeck, A. Rednikov, P. Colinet, Vapor-based interferometric measurement of local evaporation rate and interfacial temperature of evaporating droplets, Langmuir 30 (8) (2014) 2002–2008.

[27] D. Ambrose, C.H. Sprake, R. Townsend, Thermodynamic properties of organic oxygen compounds XXXIII. The vapour pressure of acetone, The Journal of Chemical Thermodynamics 6 (7) (1974) 693–700.

[28] M.H. Rausch, L. Kretschmer, S. Will, A. Leipertz, A.P. Fröba, Density, surface tension, and kinematic viscosity of hydrofluoroethers HFE-7000, HFE-7100, HFE-7200, HFE-7300, and HFE-7500, Journal of Chemical and Engineering Data 60 (12) (2015) 3759–3765.

[29] K.S. Howard, R. McAllister, Surface tension of acetone-water solutions up to their normal boiling points, AIChE Journal 3 (3) (1957) 325–329.

[30] W. Thielicke, E. Stamhuis, PIVlab–towards user-friendly, affordable and accurate digital particle image velocimetry in MATLAB, Journal of Open Research Software 2 (1) (2014) 30.

[31] R.J. Adrian, J. Westerweel, Particle Image Velocimetry, Cambridge University Press, 2011.

[32] A. Sciacchitano, Uncertainty quantification in particle image velocimetry, Measurement Science and Technology 30 (9) (2019) 092001.

[33] G.A. Lugg, Diffusion coefficients of some organic and other vapors in air, Analytical Chemistry 40 (7) (1968) 1072–1077.

[34] S. Kim, J. Kim, H.-Y. Kim, Dewetting of liquid film via vapour-mediated marangoni effect, Journal of Fluid Mechanics 872 (2019) 100–114.

[35] E.L. Cussler, Diffusion: Mass transfer in fluid systems, Cambridge University Press, 2009.

[36] B. Neél, E. Villermaux, The spontaneous puncture of thick liquid films, Journal of Fluid Mechanics 838 (2018) 192–221.

[37] J. Michell, On the direct determination of stress in an elastic solid with application to the theory of plates, Proceedings of the London Mathematical Society 31 (1899) 100–124.

[38] M.A. Wilson, A. Pohorille, Adsorption and solvation of ethanol at the water liquid - vapor interface: A molecular dynamics study, Journal of Physical Chemistry B 101 (16) (1997) 3130–3135.

[39] J. Dalton, On the expansion of elastic fluids by heat, Journal of Natural Philosophy, Chemistry, and the Arts 3 (1802) 130–134.

[40] G. Lee, H. Kim, Direct optical measurement of evaporative flux of volatile liquid droplets, Bulletin of the American Physical Society (2018).